Research Paper

Licochalcone A activation of glycolysis pathway has an anti-aging effect on human adipose stem cells

Yating Wu[1,*], Hao Wang[2,*], Jianbo Zhu[1], Haitao Shen[1], Hailiang Liu[1,2]

[1]Key Laboratory of Xinjiang Phytomedicine Resource and Utilization of Ministry of Education, College of Life Sciences, Shihezi University, Shihezi 832003, China
[2]Institute for Regenerative Medicine, Shanghai East Hospital, Tongji University School of Medicine, Shanghai 200123, China
*Equal contribution

ABSTRACT

Licochalcone A (LA) is a chalcone flavonoid of *Glycyrrhiza inflata*, which has anti-cancer, antioxidant, anti-inflammatory, and neuroprotective effects. However, no anti-aging benefits of LA have been demonstrated *in vitro* or *in vivo*. In this study, we explored whether LA has an anti-aging effect in adipose-derived stem cells (ADSCs). We performed β-galactosidase staining and measured reactive oxygen species, relative telomere lengths, and *P16*[ink4a] mRNA expression. Osteogenesis was assessed by Alizarin Red staining and adipogenesis by was assessed Oil Red O staining. Protein levels of related markers runt-related transcription factor 2 and lipoprotein lipase were also examined. RNA sequencing and measurement of glycolysis activities showed that LA significantly activated glycolysis in ADSCs. Together, our data strongly suggest that the LA have an anti-aging effect through activate the glycolysis pathway.

INTRODUCTION

Organism aging is accompanied by cell senescence caused by telomere shortening [1], increased reactive oxygen species (ROS) [2], oncogene activation [3], impaired nervous system functions, and a decline in immunity [4, 5]. The occurrence of various diseases is closely related to cell senescence [6], such as osteoporosis [7] and Parkinson's disease [5]. Lipid profiles are associated with aging. Indeed, increased uptake of specific lipids promotes longevity and ameliorates disease phenotypes *in vivo* [8]. Moreover, lipid profiles have been invaluable to identify the nine denominators of aging: telomere attrition, genome instability, epigenetic alterations, mitochondrial dysfunction, deregulated nutrient sensing, altered intercellular communication, loss of proteostasis, cellular senescence, and adult stem cell exhaustion [9].

Therefore, inhibiting replicative senescence of cells is an important consideration to improve health.

Stem cell exhaustion is a critical factor of aging. Adipose-derived stem cells (ADSCs), which are obtained from adipose tissue, exhibit a high proliferative ability, rapidly self-renew, and can be directed to differentiate into osteoblasts, fibroblasts, and nerve cells [10]. Extensive research has shown that ADSCs play major roles in aging, such as increasing the superoxide dismutase level and decreasing the malondialdehyde content of aging rats [11]. Additionally, ADSCs promote myelin sheath regeneration and reduce loss of nerve functions in mice [12]. Furthermore, injection of an Alzheimer's disease mouse model with a certain dose of ADSCs promotes microglial cell activation and nerve regeneration by ADSCs homing to the lesion site and differentiating into nerve cells [13,

14]. However, the proliferative ability of ADSCs decreases in aged animals [15] and young ADSC transplants show significantly higher bone regeneration for osteoporosis treatment [16]. Regardless, ADSCs are a suitable cell source to research aging-related problems.

Natural small molecule compounds are widely used in clinical studies. Recently, increasing attention has been focused on the molecular mechanisms related to aging controlled by an epigenetic-modulating diet with polyphenols [17]. For example, resveratrol plays an important role in anti-aging by activation of deacetylases [18], whereas quercetin induces cytochrome c expression in the brain [19].

The potential clinical applications of numerous bioactive compounds in licorice were recently investigated. Licochalcone A (LA), a characteristic chalcone extracted from the root of *Glycyrrhiza inflata* [20], has bioactive functions and exerts anti-tumor [21], antioxidant [22], anti-obesity [23], and neuroprotective effects [24] and also shows anti-cancer effects by inhibiting glioma stem cell proliferation [25]. LA also exhibits anti-obesity effects [26], inhibits thrombus formation [27], and exerts antioxidant activities by regulating nuclear factor-erythroid 2-related factor 2 (Nrf2) [28]. Another study demonstrated that LA shows anti-inflammatory effects in IL-1β-stimulated chondrocytes [29]. Furthermore, treatment with LA promotes strong osteogenic differentiation and mineralized formation of cell aggregates [30]. Thus, LA is a component of licorice with various bioactivities. Although various pharmacological activities of LA have been reported, the value of LA as an adjuvant for anti-aging remains to be determined.

In this study, we investigated whether LA had an effect on the proliferative and differentiation abilities of hADSCs and examined the underlying anti-aging mechanisms. Additionally, we determined whether treatment with LA improved cell proliferation by RNA sequencing (RNA-seq) analysis and measurement of glycolysis activities.

RESULTS

LA ameliorates replicative senescence of hADSCs

Samples of hADSCs were obtained from subcutaneous adipose tissues and the cells had been identified by our previous work [31], a characterization of the multipotency showed that a state of aging after P9 as evidenced by a gradual increase in size and irregular shape at P9 and P16. Additionally, expression of cell senescence-related molecular marker $P16^{ink4a}$ was

increased significantly, telomeres were shortened, and the number of SA-β-gal-positive cells was increased significantly at P16. Therefore, we chose aging state cells to research the anti-aging effect of LA [31].

To evaluate LA cytotoxicity, hADSC were treated with various concentrations of LA for 24 h and then evaluated for cell viability. The results indicated that LA (25 µmol) significantly increased hADSC viability compared with Ctrl treatment (p<0.05) (Supplementary Figure 1A).

Furthermore, growth curves of various passages displayed an initial lag phase of 2 days, followed by an exponential log phase from 3 to 5 days, and then cells entered a plateau phase at 6-7 days (Supplementary Figure 1B). The results showed that LA (25 µmol) promotes cell proliferation compared with Ctrl treatment on the fourth day (p<0.05).

To examine the effect of LA on senescence, we performed SA-β-gal assays. SA-β-gal staining revealed significantly fewer senescent cells in the LA treatment group compared with the Ctrl group (p<0.01) (Figure 1A).

ROS levels are important to regulate cell proliferation activity. Increased ROS levels lead to cell senescence [32]. As shown in Figure 1B, treatment with LA (25 µmol) reduced ROS levels in hADSCs compared with the Ctrl ($P<0.05$). The length of telomeres inevitably shrinks during the process of aging by telomere regulation of cell replication [33] and cell senescence [34]. Telomere shortening was suppressed in LA-treated hADSCs compared with the Ctrl ($P< 0.05$) (Figure 1C). $P16^{ink4a}$ is a marker of senescence [35] and senescence occurs by inactivation of suppressor elements, which enhances expression of p16 [36]. Western blotting showed that LA (25 µmol) treatment inhibited protein expression of $P16^{ink4a}$ in aged hADSCs compared with the Ctrl (Figure 1D).

Cell cycle arrest results in genomic instability and premature aging [37], and delayed S phase progression contributes to genome instability [38]. Cell cycle analysis showed that LA (25 µmol) treatment caused a decrease in cells in G0/G1 phase and a significant increase in S phase cells (p<0.05) compared with Ctrl cells (Figure 1E).

In normal cells, the P53 tumor suppressor maintains mitochondrial respiration. Overexpression of $P53$ drastically reduced mitochondrial Ca^{2+} transients in stimulated cells, causing mitochondrial dysfunction [39]. RT-qPCR showed that LA (25 µmol) treatment resulted in significantly reduced mRNA expression of
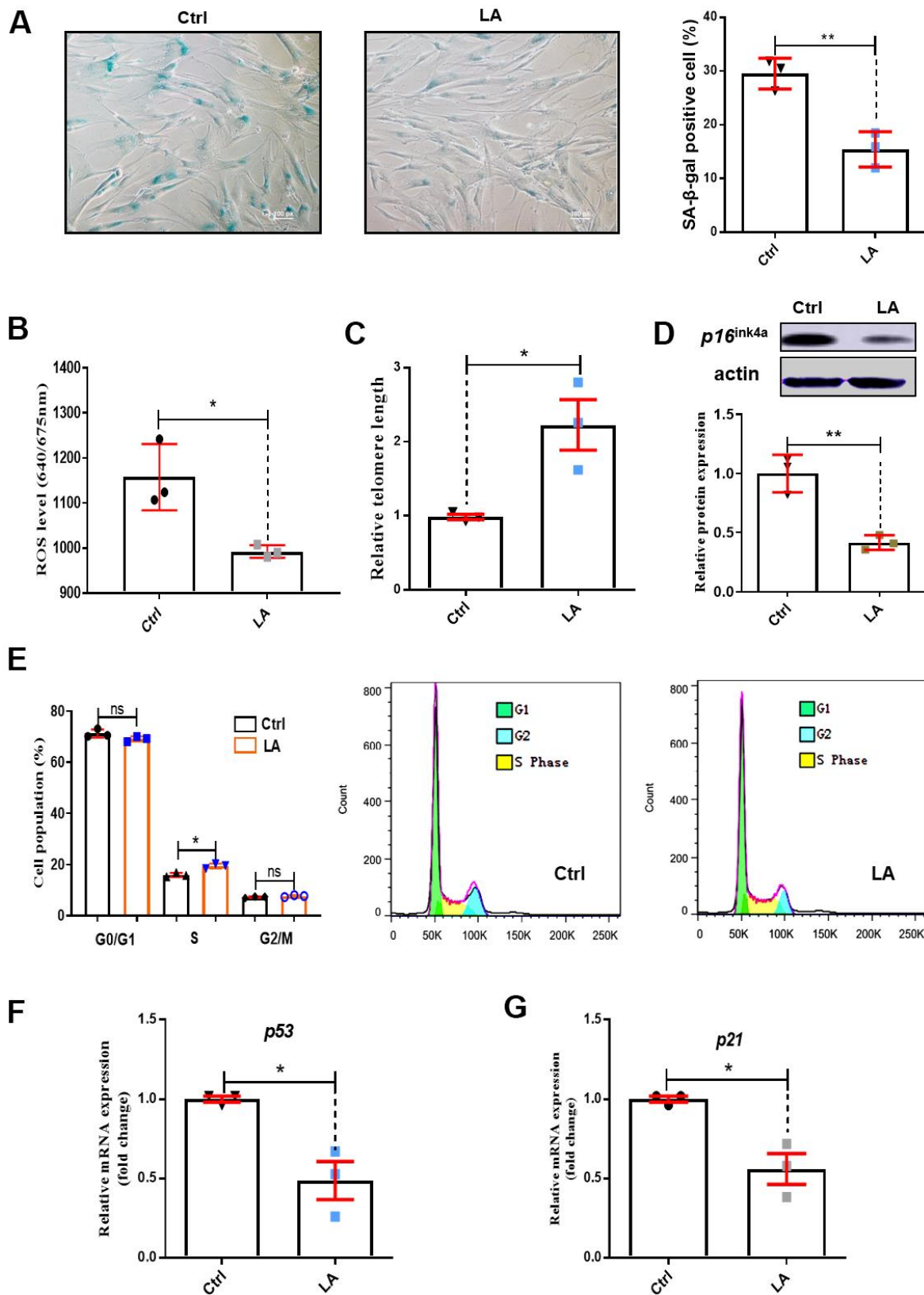
Figure 1. Effects of LA on hADSC viability. (**A**) SA-β-gal staining of hADSCs (Scale bar: 100 μm). The relative intensity of ROS was detected by a microplate reader. (**B**) Effects of LA on ROS. (**C**) Relative telomere lengths of hADSCs. (**D**) Relative protein expression of senescence gene *P16* compared with the control. (**E**) Effects of LA on cell cycle. (**F**, **G**) Relative mRNA expression of senescent genes *P21* and *P53* compared with control. Data are presented as the mean ± SD of three independent experiments. *p < 0.05, **p < 0.01 compared with untreated cells.

P53 (p<0.01) compared with Ctrl (Figure 1F). The senescence-associated secretory phenotype develops because of cellular senescence. P21 is a secretory factor that regulates senescence [40]. We found that LA (25 µmol) treatment also significantly reduced (p<0.05) the mRNA expression of *P21* compared with the Ctrl (Figure 1G).

Effect of LA on the differentiation capabilities of hADSCs

To assess the anti-aging effect of LA (25 µmol), we examined cell differentiation abilities. Osteogenic and adipogenic differentiation indicates the differentiation potentials of stem cells [41] and osteogenesis of aged MSCs is compromised significantly [42]. Unbalanced adipogenic and osteogenic differentiation of human mesenchymal stem cells promotes senescence [43].

We next examined osteogenic differentiation in hADSCs treated with LA (25 µmol) by evaluating mRNA levels of the marker genes alkaline phosphatase (*ALP*), alkaline osteocalcin (*OCN*), and runt-related transcription factor 2 (*RUNX2*) [44]. Compared with the Ctrl, LA (25 µmol) treatment increased the mRNA expressions of *ALP* (p<0.05), *OCN* (p<0.01), and *RUNX2* (p<0.01) (Figure 2A). Alizarin Red staining revealed that LA (25 µmol) promoted the formation of mineralized nodules compared with the Ctrl (Figure 2B). Western blot analysis showed that LA (25 µmol) upregulated the protein expression of RUNX2 (p<0.05) compared with the Ctrl (Figure 2C).

We also evaluated adipogenic differentiation by evaluating the mRNA levels of the marker genes peroxisome proliferator-activated receptors γ (*PPARγ*) and lipoprotein lipase (*LPL*) [45]. LA (25 µmol) treatment decreased the mRNA expression of *PPARγ* (p<0.01) and *LPL* (p<0.05) compared with the Ctrl (Figure 2D). Oil Red O staining showed that LA (25 µmol) treatment resulted in fewer fat droplets compared with the Ctrl (Figure 2E). Western blot analysis showed that LA (25 µmol) downregulated the protein expression of LPL (p<0.01) compared with the Ctrl (Figure 2F). These results demonstrated that LA (25 µmol) promotes hADSC differentiation toward osteogenesis and attenuates adipogenic differentiation.

Effect of LA on glycolysis/gluconeogenesis pathways in hADSCs

On the basis of RNA-seq to analyze the specific mechanism, a classification map of KEGG pathway analysis revealed that 4 signaling pathways related to cell growth and death were regulated by LA (25 µmol) (Figure 3A). Furthermore, a bubble diagram showed that glycolysis/gluconeogenesis signaling pathways were regulated by LA (Figure 3B) and a heatmap showed differentially expressed genes related to glycolysis/gluconeogenesis signaling pathways (Figure 3C). Heatmap analysis showed that the expressions of *GAPDH*, *MMP14*, *PKM*, *MMP17*, and *PFKP* genes, which are related to the glycolysis/gluconeogenesis signaling pathway, were upregulated in the LA group compared with the Ctrl group. Examination of differentially expressed genes revealed 21 upregulated genes and 51 downregulated genes in the LA -treated group compared with the Ctrl group (Figure 3D). Furthermore, gene set enrichment analysis (GSEA) of the differentially expressed genes revealed that LA treatment activated the glycolysis/gluconeogenesis signaling pathways (Figure 3E).

To verify the RNA-seq results, we examined the mRNA levels of *PKM*, *PFKP*, and *GAPDH* in hADSCs treated with LA (25 µmol). Treatment with LA significantly increased the mRNA expressions of *PKM* (p<0.05), *PFKP* (p<0.05), and *GAPDH* (p<0.01) in hADSCs compared with the Ctrl group (Figure 3F). Western blot analysis also showed that LA upregulated the protein expression of *MMP*14 (p<0.01), *PFKP* (p<0.01) compared with the Ctrl and LA cannot regulate the protein expression of *PKM* (Supplementary Figure 2).

LA promotes hADSC proliferation by activating the glycolysis pathway

To evaluate the effect of LA on glycolysis/gluconeogenesis pathways in hADSCs, we used extracellular flux analyzes to monitor the extracellular acidification rate (ECAR) and oxygen consumption rate (OCR) [46, 47], which indicated glycolysis pathway activity and mitochondrial respiration, respectively.

Following LA treatment of hADSCs, glucose consumption was increased (Figure 4A). ECAR in hADSCs at each phase in the glycolysis pathway showed that basal, glucose, oligomycin, and 2-DG (2-Deoxy-D-glucose, one of the glycolysis inhibitors) phases were significantly higher in LA1 and LA2 groups than in the Ctrl (*P*<0.01) (Figure 4B). Additionally, when treated with LA (25 µmol), the relationship between ECAR and OCR showed a positive correlation and was higher than in the Ctrl (Figure 4C). Glycolysis levels showed that LA activated the glycolysis pathway by significantly improving ECAR and OCR in aged hADSCs compared with the Ctrl.
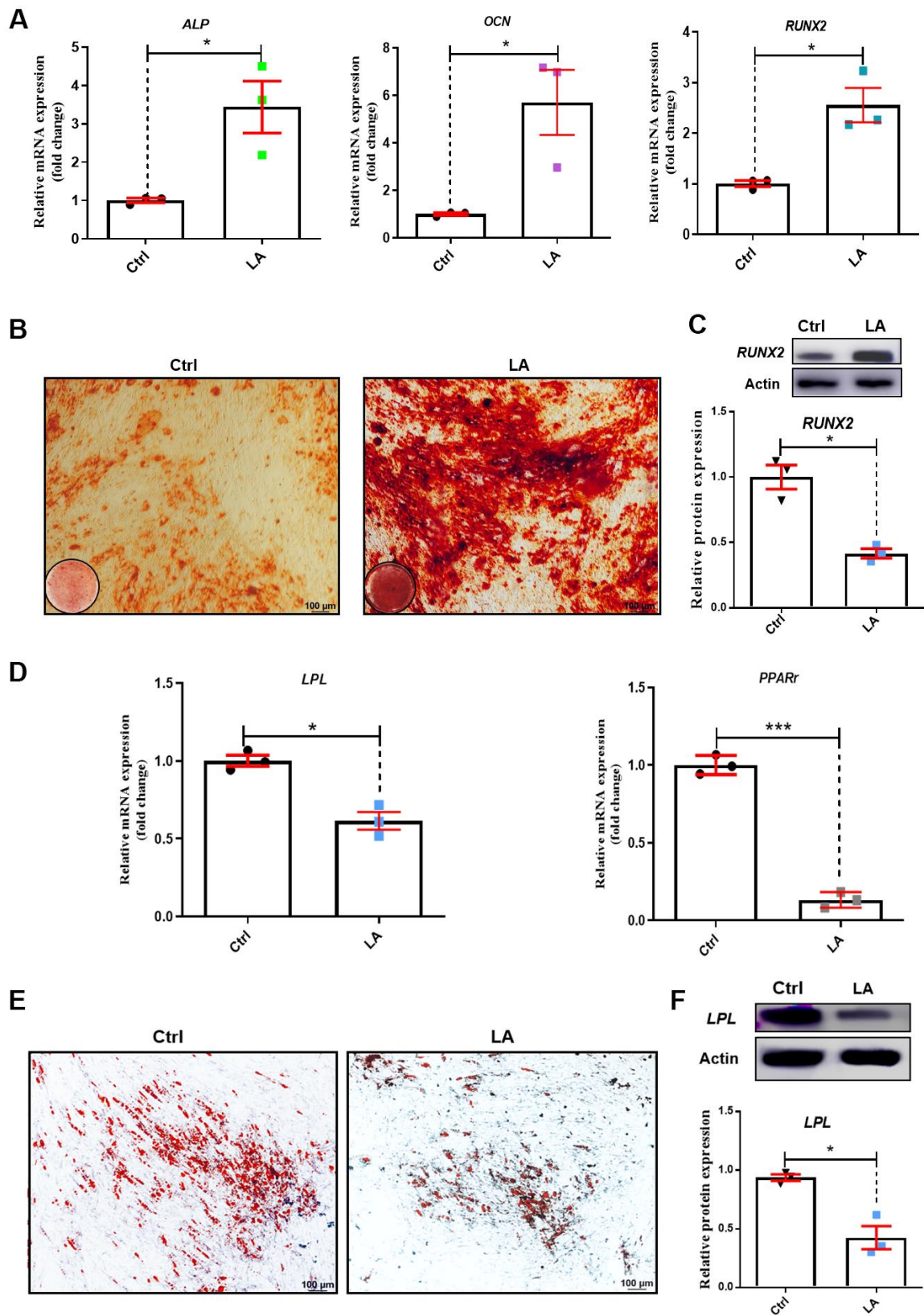
Figure 2. Effects of LA on hADSC differentiation ability. (**A**) qRT-PCR of mRNA levels of the osteogenic differentiation markers *ALP*, *OCN*, and *RUNX2*. (**B**) Alizarin Red staining of hADSCs. (**C**) Western blot in hADSCs treated as indicated. (**D**) qRT-PCR of mRNA levels of the adipogenic differentiation markers *PPARr* and *LPL*. (**E**) Oil Red O staining of hADSCs. (**F**) Western blot in hADSCs treated as indicated. Data are presented as the mean ± SD of three independent experiments. *p < 0.05, **p < 0.01, ***p < 0.001 compared with untreated cells.

Previous RNA-seq data suggested that LA can increases the expression of *GAPDH*, a critical regulation enzyme in the glycolysis pathway, and the upregulation of GAPDH expression can activate glycolysis progression [48]. Western blot analysis showed that GAPDH protein level was increased in hADSCs treated with LA (p<0.05) compared with the Ctrl (Figure 4D).

Other research found that AMPK (AMP-activated protein kinase) has been shown to regulate the senescence [49], which have reduced the expression of the epigenetic factor p-AMPK (phospho-AMP-activated protein kinase) in aged mice [50]. AMPK can mediate increase of glycolysis in human cells [51]. Western blot analysis also showed that LA (25 µmol) upregulated the protein expression of *p-AMPK* (p<0.01) compared with the Ctrl and cannot regulate the protein expression of *AMPK* (Supplementary Figure 3).

DISCUSSIONS

Young hADSCs are an ideal source of adult stem cells in clinical applications. However, the continuous culture of mesenchymal stem cells results in cell senescence. In this study, we examined the potential anti-aging effects of LA (25 µmol) on senescent hADSCs. Related evaluations confirm the regulation of LA on aging. The expression of *P16INK4A*, which regulates senescence, was downregulated by LA [52]. ROS levels are increased in aging cells, and increased ROS levels inhibit cell proliferation [53]. Our results showed that LA decreased the ROS level in hADSCs. Telomeres become shorter in senescent cells [54]. LA can protect telomeres from shortening in hADSCs during proliferation. Osteogenic and adipogenic differentiation is also a critical aging indicator [55]. During mesenchymal stem cell aging, bone mass decreases and bone marrow adiposity increases [56].

We performed osteogenic and adipogenic differentiation assays and found that LA (25 µmol) promoted osteogenesis differentiation and attenuated adipogenic differentiation of hADSCs. Although the four signaling pathways regulated by LA through RNA-seq analysis mainly involved cell growth and death but not osteogenic and adipogenic differentiation. This may
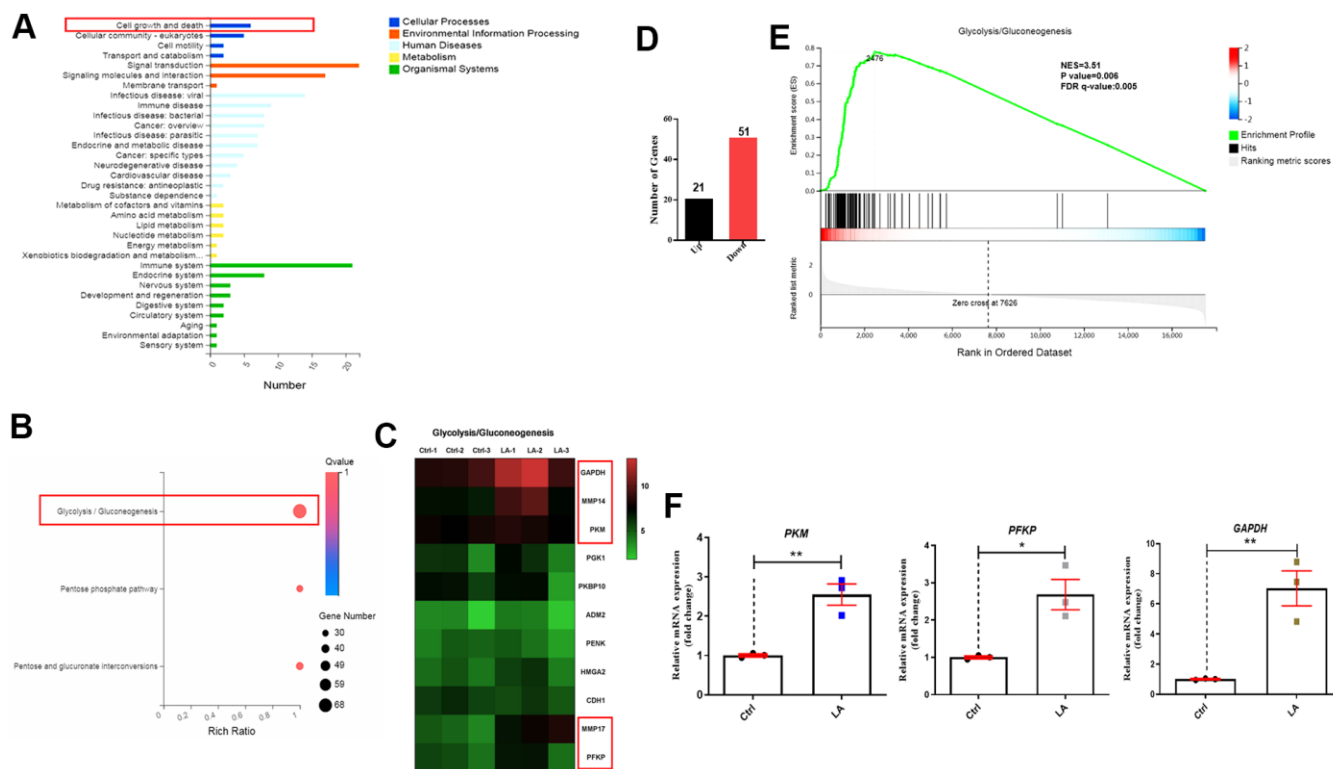

Figure 3. Mechanism of LA in regulation of hADSC proliferation determined by RNA-seq. (**A**) Classification map of KEGG pathway analysis. (**B**) Bubble diagram of glycolysis/gluconeogenesis signaling pathways regulated by LA. (**C**) Heatmap of differentially expressed genes related to glycolysis/gluconeogenesis signaling pathways. (**D**) The differentially expressed genes. (**E**) Enrichment plots of gene expression signatures for the glycolysis/gluconeogenesis signaling pathway. (**F**) qRT-PCR of the relative mRNA expression of *PKM*, *PFKP*, and *GAPDH* in LA-treated hADSCs. Data are presented as the mean ± SD of three independent experiments. Statistical significance was determined by the unpaired t-test. *p < 0.05, **p < 0.01 compared with the Ctrl.

be that the increase of osteogenic differentiation and the decrease of adipogenic differentiation in hADSCs caused by LA treatment is only a phenotype in cellular senescence.

Our RNA-seq results suggest that LA (25 µmol) activates the glycolysis signaling pathway by promoting *GAPDH*, *PKM*, *MMP14*, and *PFKP* gene expression. The glycolysis pathway is linked to cell growth and proliferation [57], so activation of the glycolysis pathway promotes cell viability and ameliorates aging [58]. *GAPDH*, *PKM*, *MMP14*, and *PFKP* are important factors in the glycolysis signaling pathway. For example, GAPDH activates the glycolysis pathway [59]. Increased expression of the glycolysis enzyme PKM facilitates a metabolic shift to glycolysis [60], and PFKP plays important roles in cellular glucose metabolism [61]. The results showed that LA activates the *p-AMPK*, which also involved in the senescence. Glycolysis inhibitor blocked LA-induced *AMPK*

phosphorylation (Supplementary Figure 4A), and inhibition of Glycolysis blocked LA- attenuate fewer senescent cells (Supplementary Figure 4B) and expression of p16 gene from hADSCs (Supplementary Figure 4C).

In conclusion, our results suggest that the anti-aging effects of LA (25 µmol) are associated with induction of the glycolysis pathway. As is known to all, glycolysis is a critical pathway in glucose metabolism that provides intermediates for energy generation [62]. Such as upregulation of glycolysis is a major characteristic of provides energy to support rapid proliferation [63]. Glycolysis also regulates the activation of fibrogenesis in the aged lung *in vivo* and *in vitro* [57]. So, glycolysis is linked to cell growth and the findings showed the anti-aging property of LA by activating the glycolysis pathway. These findings may have broad implications for therapeutic that LA has an anti-aging effect on human adipose stem cells.
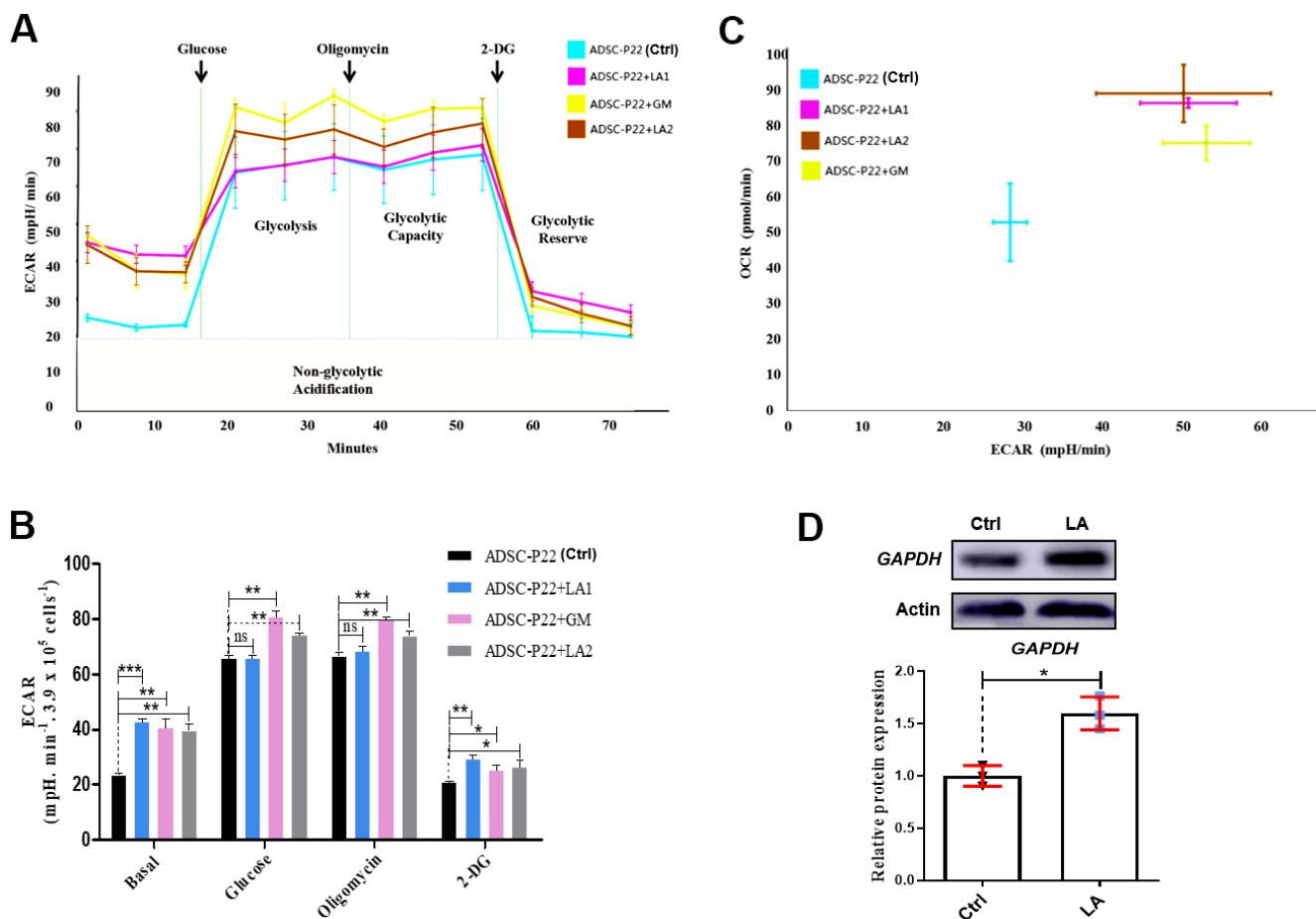
Figure 4. Measurements of glycolysis activities in hADSCs. (**A**) ECAR in hADSCs at each phase of the glycolysis pathway. (**B**) Statistical analysis of ECAR at each phase. (**C**) Relationship between ECAR and OCR in the glycolysis pathway of hADSCs. GM: Metformin. (**D**) Western blotting of GAPDH protein expression. Data are presented as the mean ± SD of three independent experiments. Statistical significance was determined by the unpaired t-test. *p < 0.05, **p < 0.01, ***p < 0.001 compared with the Ctrl.

MATERIALS AND METHODS

Cell culture and viability assay

LA (C21H22O4; MW: 338; ≥98% pure, HPLC grade) was purchased from Chengdu Push Biotechnology Co. Ltd. (Sichuan, China) and stored at 2–8° C in a dark, dry place. The stock solution concentration was 100 mmol in dimethyl sulfoxide (DMSO). The final DMSO concentration did not exceed 0.1% in the culture medium. hADSCs at passage (P) 22 (late passage) were cultured in a humidified atmosphere with 5% CO_2 at 37° C in DMEM/F12 (Thermo Fisher Scientific, Waltham, MA, USA) supplemented with 10% FBS and 100 U/mL penicillin and streptomycin.

Cell viability and growth kinetics were measured by CCK-8 assays. Briefly, cells were seeded in 96-well culture plates and treated for 24 h with various concentrations of LA (0, 25, 50, and 100 µmol for the cell viability assay; 25 µmol for the growth kinetics assay). Next, 10 µL CCK-8 solution was added to each well, followed by incubation at 37° C for 2 h. Cell viability was measured using a microplate reader by recording the absorbance of each well at 450 nm.

SA-β-gal assay

hADSCs were cultured in 24-well plates overnight and then treated with 25 µmol LA or the vehicle control for 24 h. Next, the cells were fixed and treated with SA-β-gal kit solution. Cell staining was examined by fluorescence microscopy.

ROS assay

hADSCs were treated with 25 µmol LA or the vehicle control for 24 h and then incubated with ROS reagent in the dark at room temperature for 30 minutes (min). ROS levels were determined using a multi-mode microplate reader.

qRT-PCR analysis

Telomere lengths in hADSCs were measured by qRT-PCR. hADSCs were seeded in six-well plates and treated with 25 µmol LA and the vehicle control (Ctrl) for 24 h. Briefly, total mRNA was extracted using Trizol (Thermo Fisher Scientific) and then reverse transcribed into cDNA using a reverse transcription kit. Total DNA was extracted using a DNA extraction kit. The PCR protocol was as follows: predenaturation at 95° C for 3 min followed by 43 cycles of denaturation at 95° C for 10 s, annealing at 55° C for 30 s, and extension at 72° C for 30 s. *36B4* was used as a Ctrl. qRT-PCR was performed using the Taq-Man real-time PCR system (Thermo

Fisher Scientific) and SYB-Green real-time PCR system (TaKaRa). Relative gene expression levels were normalized to *ACTB* and calculated by the $2^{-\Delta\Delta CT}$ method. Primer sequences are listed in Table 1.

Osteogenic and adipogenic differentiations assays

Briefly, cells were cultured in DMEM/F12 containing 25 µmol LA or Ctrl. At 70% confluence, cells were treated with OriCell™ differentiation media with 25 µmol LA maintained throughout the differentiation period. Alizarin Red staining was performed on day 25 for osteogenesis and Oil Red O staining on day 14 for adipogenesis. Images were obtained by microscopy.

RNA-seq analysis

RNA-seq was performed independently and uniformly on hADSCs treated with LA (25 µmol) or Ctrl in duplicate and cultured for 6 days in a humidified atmosphere with 5% CO2 at 37° C in DMEM/F12 supplemented with 10% FBS and 100 U/mL penicillin and streptomycin. Clean reads were aligned to the reference gene sequence using bowtie-2 and the gene expression levels of each sample were calculated. Differentially expressed gene (DEG) detection was conducted by the DEG seq method [62]. The statistical results were based on the ma-plot method. The number of reads of specific genes obtained from the sample was randomly sampled, and then *p*-values were calculated in accordance with the normal distribution and corrected to q-values. To improve the accuracy of DEGs, genes with a different multiple of more than double and a q-value of ≤0.001 were defined and screened as significant DEGs. RNA sequencing data generated from this study have been deposited in NCBI GEO (https://www.ncbi.nlm.nih.gov/geo) under the accession number GSE144105.

Western blot analysis

Briefly, hADSC were treated with 25 µmol LA or Ctrl for 24 h and 48 h (or 80 h) then lysed using RIPA buffer containing protease and phosphatase inhibitors at 4° C, followed by centrifugation for 10 min. The supernatant was collected and sample buffer (5×) was added at a ratio of 5:1. Samples were mixed well and boiled for 10 min, followed by storage at −40° C. Proteins were separated by 10% SDS polyacrylamide gel electrophoresis and transferred to PVDF membranes that were blocked by incubation with 2.5% dry skim milk, followed by overnight incubation with primary antibodies diluted in 2.5% dry skim milk at 4° C.

The following antibodies were used: monoclonal rabbit anti-*RUNX2*, anti-*LPL*, anti-P16ink4a, anti-*GAPDH*, anti-*MMP14*, anti-*PKM*, anti-*PFKP*, anti-*AMPK*, anti-*p*-

Table 1. The primer of qRT-PCR.

Gene	F (5'-3')	R (5'-3')
h-P21	TTAGCAGCGGAACAAGGA	AAGACAACTACTCCCAGCCC
h-P53	TGCATTTTCACCCCACCCTT	ACACAGGTGGCAGCAAAGTT
h-ALP	GATGGCCTGAACCTCATCGA	AGTTCGGTCCGGTTCCAGAT
h-RUNX2	TGGCCGGGAATGATGAGA	TGAAACTCTTGCCTCGTCCG
h-OCN	GGACTGTGACGAGTTGGCTGAC	TGCCTGGAGAGGAGCAGAACTG
h-LPL	TGTATGAGAGTTGGGTGCCAAA	GCCAGTCCACCACAATGACAT
h-PPARr	TGCAAGGGTTTCTTCCGGA	GCAAGGCATTTCTGAAACCG
h-PFKP	CGGAAGTTCCTGGAGCACCTCTC	AAGTACACCTTGGCCCCCACGTA
h-GAPDH	ATCAGCAATGCCTCCTGCAC	TGGTCATGAGTCCTTCCACG
h-PKM	ATGTCGAAGCCCCATAGTGAA	TGGGTGGTGAATCAAGTCCA
h-actin	ACCCACACTGTGCCCATCT	ATGTCACGCACGATTTCCC
h-telomere	GGTTTTTGAGGGTGAGGGTGAGGGTG AGGGTGAGGGT	TCCCGACTATCCCTATCCCTATCCCTATC CCTATCCCTA
h-36B4	CAGCAAGTGGGAAGGTGTAATCC	CCCATTCTATCATCAACGGGTACAA

AMPK (Abcam) at 1:1000 dilutions. The blots were then incubated with the secondary mouse or rabbit antibodies at room temperature for 1 h. Proteins were detected using the BioSpectrum 600 system. The western blots repeated 3 independent experiments.

Measurement of glycolysis activities

The oxygen consumption rate (OCR; pmoles/min) and extracellular acidification rate (ECAR; mpH/min) were measured using Seahorse XF96 extracellular flux analyzers (Seahorse Bioscience, Billerica, MA, USA) in accordance with the manufacturer's instructions [63]. hADSCs were seeded in an XF96 cell culture microplate. Twenty-four hours (h) later, DMEM/F12 medium was changed to Agilent Seahorse XF base medium (Agilent Technologies) supplemented with GlutaMAX™ (Thermo Fisher Scientific). The cells were cultured for 1 h in a CO_2-free 37° C incubator and then subjected to a Seahorse XF Cell Mito Stress Test or Seahorse XF Glycolysis Stress Test. LA concentrations were 6.25 µmol (LA1) and 25 µmol (LA2) for the glycolysis test. Measurements were recorded at the intervals indicated in the test protocols.

Statistical analysis

Statistical analysis was performed using GraphPad Prism 5.0. Data are expressed as the mean ± standard deviation (SD). Statistical comparisons of two groups were made by the unpaired t-test. Statistical comparisons of more than two groups were made by analysis of variance (ANOVA). A two-tailed *P*-value of $P<0.05$ was considered statistically significant and $P<0.01$ was considered extremely statistically significant.

Abbreviations

LA: Licochalcone A; ADSC: Adipose-derived stem cells; DEGs: Differentially expressed genes; ECAR: Extracellular acidification rate; OCR: Oxygen consumption rate; *GAPDH:* Glyceraldehyde-3-phosphate dehydrogenase; H: Hour; Min: Minutes (min); hADSC: Human adipose-derived stem cells; *RUNX2:* Runt-related transcription factor 2; *LPL:* Lipoprotein lipase; *PPARγ:* peroxisome proliferator-activated receptors γ; *ALP:* Alkaline phosphatase; *OCN:* Alkaline osteocalcin; *PKM:* Pyruvate kinase muscle type; *MMP*14: Matrix metalloproteinase 14; *PFKP:* Platelet isoform of phosphofructokinase; RNA-seq: RNA sequencing; ROS: Reactive oxygen species; SA-β-gal: Senescence-associated β-galactosidase.

AUTHOR CONTRIBUTIONS

All authors participated in data acquisition. Y.W. and H.W. performed experiments. Y.W. and H.L. analyzed data. H.L. supervised the project., J. Z., H. S and H.L designed the project. Y.W. and H. L. wrote the paper.

CONFLICTS OF INTEREST

The authors declare that they have no conflicts of interest.

FUNDING

REFERENCES

1. Bayne S, Li H, Jones ME, Pinto AR, van Sinderen M, Drummond A, Simpson ER, Liu JP. Estrogen deficiency reversibly induces telomere shortening in mouse granulosa cells and ovarian aging *in vivo*. Protein Cell. 2011; 2:333–46.
https://doi.org/10.1007/s13238-011-1033-2
PMID:21574023

2. Callaway DA, Jiang JX. Reactive oxygen species and oxidative stress in osteoclastogenesis, skeletal aging and bone diseases. J Bone Miner Metab. 2015; 33:359–70.
https://doi.org/10.1007/s00774-015-0656-4
PMID:25804315

3. Szabo E, Phelan SA. Abstract 5481: role and regulation of Peroxiredoxin antioxidant proteins in K562 leukemia cells. Cancer Res. 2017 (Suppl 13); 77:5481.
https://doi.org/10.1158/1538-7445.AM2017-5481

4. Kim Y, Griffin JM, Nor MN, Zhang J, Freestone PS, Danesh-Meyer HV, Rupenthal ID, Acosta M, Nicholson LF, O'Carroll SJ, Green CR. Tonabersat Prevents Inflammatory Damage in the Central Nervous System by Blocking Connexin43 Hemichannels. Neurotherapeutics. 2017; 14:1148–65.
https://doi.org/10.1007/s13311-017-0536-9
PMID:28560708

5. Kustrimovic N, Marino F, Cosentino M. Peripheral Immunity, Immunoaging and Neuroinflammation in Parkinson's Disease. Curr Med Chem. 2019; 26:3719–53.
https://doi.org/10.2174/0929867325666618100916104
8 PMID:30306855

6. Bonzón-Kulichenko E, Moltó E, Pintado C, Fernández A, Arribas C, Schwudke D, Gallardo N, Shevchenko A, Andrés A. Changes in Visceral Adipose Tissue Plasma Membrane Lipid Composition in Old Rats Are Associated With Adipocyte Hypertrophy With Aging. J Gerontol A Biol Sci Med Sci. 2018; 73:1139–46.
https://doi.org/10.1093/gerona/gly081
PMID:29668887

7. Farr JN, Xu M, Weivoda MM, Monroe DG, Fraser DG, Onken JL, Negley BA, Sfeir JG, Ogrodnik MB, Hachfeld CM, LeBrasseur NK, Drake MT, Pignolo RJ, et al. Targeting cellular senescence prevents age-related bone loss in mice. Nat Med. 2017; 23:1072–79.
https://doi.org/10.1038/nm.4385
PMID:28825716

8. Papsdorf K, Brunet A. Linking Lipid Metabolism to Chromatin Regulation in Aging. Trends Cell Biol. 2019; 29:97–116.
https://doi.org/10.1016/j.tcb.2018.09.004
PMID:30316636

9. Vermeij WP, Hoeijmakers JH, Pothof J. Genome Integrity in Aging: Human Syndromes, Mouse Models, and Therapeutic Options. Annu Rev Pharmacol Toxicol. 2016; 56:427–45.
https://doi.org/10.1146/annurev-pharmtox-010814-124316 PMID:26514200

10. Caplan AI, Dennis JE. Mesenchymal stem cells as trophic mediators. J Cell Biochem. 2006; 98:1076–84.
https://doi.org/10.1002/jcb.20886
PMID:16619257

11. Yang C, Du YK, Wang J, Luan P, Yang QL, Huang WH, Yuan L. Transplanted Adipose-Derived Stem Cells Ameliorate Testicular Dysfunction In A D-Galactose-Induced Aging Rat Model. J Cell Physiol. 2015; 230:2403–14.
https://doi.org/10.1002/jcp.24970
PMID:25728126

12. Gerdoni E, Gallo B, Casazza S, Musio S, Bonanni I, Pedemonte E, Mantegazza R, Frassoni F, Mancardi G, Pedotti R, Uccelli A. Mesenchymal stem cells effectively modulate pathogenic immune response in experimental autoimmune encephalomyelitis. Ann Neurol. 2007; 61:219–27.
https://doi.org/10.1002/ana.21076
PMID:17387730

13. Oddo S, Caccamo A, Kitazawa M, Tseng BP, LaFerla FM. Amyloid deposition precedes tangle formation in a triple transgenic model of Alzheimer's disease. Neurobiol Aging. 2003; 24:1063–70.
https://doi.org/10.1016/j.neurobiolaging.2003.08.012
PMID:14643377

14. Gu R, Hou X, Pang R, Li L, Chen F, Geng J, Xu Y, Zhang C. Human adipose-derived stem cells enhance the glutamate uptake function of GLT1 in SOD1(G93A)-bearing astrocytes. Biochem Biophys Res Commun. 2010; 393:481–86.
https://doi.org/10.1016/j.bbrc.2010.02.029
PMID:20152807

15. Bae HS, Son HY, Son Y, Kim S, Hong HS, Park JU. Assessing biological aging following systemic administration of bFGF-supplemented adipose-derived stem cells with high efficacy in an experimental rat model. Exp Ther Med. 2019; 17:2407–16.
https://doi.org/10.3892/etm.2019.7251
PMID:30906427

16. Liu HY, Chiou JF, Wu AT, Tsai CY, Leu JD, Ting LL, Wang MF, Chen HY, Lin CT, Williams DF, Deng WP. The effect of diminished osteogenic signals on reduced osteoporosis recovery in aged mice and the potential therapeutic use of adipose-derived stem cells. Biomaterials. 2012; 33:6105–12.
https://doi.org/10.1016/j.biomaterials.2012.05.024
PMID:22698723

17. Cătană CS, Atanasov AG, Berindan-Neagoe I. Natural products with anti-aging potential: Affected targets and molecular mechanisms. Biotechnol Adv. 2018; 36:1649–56.
https://doi.org/10.1016/j.biotechadv.2018.03.012
PMID:29597027

18. Hou X, Rooklin D, Fang H, Zhang Y. Resveratrol serves as a protein-substrate interaction stabilizer in human SIRT1 activation. Sci Rep. 2016; 6:38186.
https://doi.org/10.1038/srep38186 PMID:27901083

19. Suliman HB, Piantadosi CA. Mitochondrial Quality Control as a Therapeutic Target. Pharmacol Rev. 2016; 68:20–48.
https://doi.org/10.1124/pr.115.011502
PMID:26589414

20. Song W, Qiao X, Chen K, Wang Y, Ji S, Feng J, Li K, Lin Y, Ye M. Biosynthesis-Based Quantitative Analysis of 151 Secondary Metabolites of Licorice To Differentiate Medicinal Glycyrrhiza Species and Their Hybrids. Anal Chem. 2017; 89:3146–53.
https://doi.org/10.1021/acs.analchem.6b04919
PMID:28192986

21. Huang WC, Su HH, Fang LW, Wu SJ, Liou CJ. Licochalcone A Inhibits Cellular Motility by Suppressing E-cadherin and MAPK Signaling in Breast Cancer. Cells. 2019; 8:218.
https://doi.org/10.3390/cells8030218 PMID:30841634

22. Huang WC, Liu CY, Shen SC, Chen LC, Yeh KW, Liu SH, Liou CJ. Protective Effects of Licochalcone A Improve Airway Hyper-Responsiveness and Oxidative Stress in a Mouse Model of Asthma. Cells. 2019; 8:617.
https://doi.org/10.3390/cells8060617 PMID:31226782

23. Lee HE, Yang G, Han SH, Lee JH, An TJ, Jang JK, Lee JY. Anti-obesity potential of Glycyrrhiza uralensis and licochalcone A through induction of adipocyte browning. Biochem Biophys Res Commun. 2018; 503:2117–23.
https://doi.org/10.1016/j.bbrc.2018.07.168
PMID:30093114

24. Huang B, Liu J, Ju C, Yang D, Chen G, Xu S, Zeng Y, Yan X, Wang W, Liu D, Fu S. Licochalcone A Prevents the Loss of Dopaminergic Neurons by Inhibiting Microglial Activation in Lipopolysaccharide (LPS)-Induced Parkinson's Disease Models. Int J Mol Sci. 2017; 18:2043.
https://doi.org/10.3390/ijms18102043
PMID:28937602

25. Kuramoto K, Suzuki S, Sakaki H, Takeda H, Sanomachi T, Seino S, Narita Y, Kayama T, Kitanaka C, Okada M. Licochalcone A specifically induces cell death in glioma stem cells via mitochondrial dysfunction. FEBS Open Bio. 2017; 7:835–44.
https://doi.org/10.1002/2211-5463.12226
PMID:28593138

26. Liou CJ, Lee YK, Ting NC, Chen YL, Shen SC, Wu SJ, Huang WC. Protective Effects of Licochalcone A Ameliorates Obesity and Non-Alcoholic Fatty Liver Disease Via Promotion of the Sirt-1/AMPK Pathway in Mice Fed a High-Fat Diet. Cells. 2019; 8:447.
https://doi.org/10.3390/cells8050447 PMID:31083505

27. Guo W, Liu B, Yin Y, Kan X, Gong Q, Li Y, Cao Y, Wang J, Xu D, Ma H, Fu S, Liu J. Licochalcone A Protects the Blood-Milk Barrier Integrity and Relieves the Inflammatory Response in LPS-Induced Mastitis. Front Immunol. 2019; 10:287.
https://doi.org/10.3389/fimmu.2019.00287
PMID:30858849

28. Lv H, Xiao Q, Zhou J, Feng H, Liu G, Ci X. Licochalcone A Upregulates Nrf2 Antioxidant Pathway and Thereby Alleviates Acetaminophen-Induced Hepatotoxicity. Front Pharmacol. 2018; 9:147.
https://doi.org/10.3389/fphar.2018.00147
PMID:29628888

29. Jia T, Qiao J, Guan D, Chen T. Anti-Inflammatory Effects of Licochalcone A on IL-1β-Stimulated Human Osteoarthritis Chondrocytes. Inflammation. 2017; 40:1894–902.
https://doi.org/10.1007/s10753-017-0630-5
PMID:28756519

30. Kim SN, Bae SJ, Kwak HB, Min YK, Jung SH, Kim CH, Kim SH. *In vitro* and *in vivo* osteogenic activity of licochalcone A. Amino Acids. 2012; 42:1455–65.
https://doi.org/10.1007/s00726-011-0901-7
PMID:21468757

31. Shen J, Zhu X, Liu H. MiR-483 induces senescence of human adipose-derived mesenchymal stem cells through IGF1 inhibition. Aging (Albany NY). 2020; 12:15756–70.
https://doi.org/10.18632/aging.103818
PMID:32805717

32. Davalli P, Mitic T, Caporali A, Lauriola A, D'Arca D. ROS, Cell Senescence, and Novel Molecular Mechanisms in Aging and Age-Related Diseases. Oxid Med Cell Longev. 2016; 2016:3565127.
https://doi.org/10.1155/2016/3565127
PMID:27247702

33. Liu J, Wang L, Wang Z, Liu JP. Roles of Telomere Biology in Cell Senescence, Replicative and Chronological Ageing. Cells. 2019; 8:54.
https://doi.org/10.3390/cells8010054 PMID:30650660

34. Zhu Y, Liu X, Ding X, Wang F, Geng X. Telomere and its role in the aging pathways: telomere shortening, cell senescence and mitochondria dysfunction. Biogerontology. 2019; 20:1–16.

https://doi.org/10.1007/s10522-018-9769-1
PMID:30229407

35. Malaise O, Tachikart Y, Constantinides M, Mumme M, Ferreira-Lopez R, Noack S, Krettek C, Noël D, Wang J, Jorgensen C, Brondello JM. Mesenchymal stem cell senescence alleviates their intrinsic and seno-suppressive paracrine properties contributing to osteoarthritis development. Aging (Albany NY). 2019; 11:9128–46.
https://doi.org/10.18632/aging.102379
PMID:31644429

36. Rayess H, Wang MB, Srivatsan ES. Cellular senescence and tumor suppressor gene p16. Int J Cancer. 2012; 130:1715–25.
https://doi.org/10.1002/ijc.27316 PMID:22025288

37. Cho JG, Choi JS, Lee JH, Cho MG, Kim HS, Noh HD, Lim KH, Park B, Kim JO, Park SG. MED28 Over-Expression Shortens the Cell Cycle and Induces Genomic Instability. Int J Mol Sci. 2019; 20:1746.
https://doi.org/10.3390/ijms20071746
PMID:30970566

38. Wang WL, Huang HC, Kao SH, Hsu YC, Wang YT, Li KC, Chen YJ, Yu SL, Wang SP, Hsiao TH, Yang PC, Hong TM. Slug is temporally regulated by cyclin E in cell cycle and controls genome stability. Oncogene. 2015; 34:1116–25.
https://doi.org/10.1038/onc.2014.58 PMID:24662826

39. Ottolini D, Calì T, Negro A, Brini M. The Parkinson disease-related protein DJ-1 counteracts mitochondrial impairment induced by the tumour suppressor protein p53 by enhancing endoplasmic reticulum-mitochondria tethering. Hum Mol Genet. 2013; 22:2152–68.
https://doi.org/10.1093/hmg/ddt068
PMID:23418303

40. Okuda R, Aoshiba K, Matsushima H, Ogura T, Okudela K, Ohashi K. Cellular senescence and senescence-associated secretory phenotype: comparison of idiopathic pulmonary fibrosis, connective tissue disease-associated interstitial lung disease, and chronic obstructive pulmonary disease. J Thorac Dis. 2019; 11:857–64.
https://doi.org/10.21037/jtd.2019.02.11
PMID:31019774

41. Huang T, Liu R, Fu X, Yao D, Yang M, Liu Q, Lu WW, Wu C, Guan M. Aging Reduces an ERRalpha-Directed Mitochondrial Glutaminase Expression Suppressing Glutamine Anaplerosis and Osteogenic Differentiation of Mesenchymal Stem Cells. Stem Cells. 2017; 35:411–24.
https://doi.org/10.1002/stem.2470 PMID:27501743

42. Yang YK, Ogando CR, Wang See C, Chang TY, Barabino GA. Changes in phenotype and differentiation potential of human mesenchymal stem cells aging *in vitro*. Stem Cell Res Ther. 2018; 9:131.
https://doi.org/10.1186/s13287-018-0876-3
PMID:29751774

43. Cheng H, Qiu L, Zhang H, Cheng M, Li W, Zhao X, Liu K, Lei L, Ma J. Arsenic trioxide promotes senescence and regulates the balance of adipogenic and osteogenic differentiation in human mesenchymal stem cells. Acta Biochim Biophys Sin (Shanghai). 2011; 43:204–209.
https://doi.org/10.1093/abbs/gmq130
PMID:21257625

44. Fei DD, Li B, Gao F, Liu AQ, Jin Y, Wang QT. [Effects of cell-to-cell communication and histone acetyltransferase on the change of osteogenic differentiation ability among single-cell clones from healthy periodontium with heterogeneity of osteogenic differentiation abilities]. Zhonghua Kou Qiang Yi Xue Za Zhi. 2017; 52:283–88.
https://doi.org/10.3760/cma.j.issn.1002-0098.2017.05.005 PMID:28482443

45. Zhang Y, Wang Y, Wang H, Ma X, Zan L. MicroRNA-224 impairs adipogenic differentiation of bovine preadipocytes by targeting LPL. Mol Cell Probes. 2019; 44:29–36.
https://doi.org/10.1016/j.mcp.2019.01.005
PMID:30703449

46. Millman JR, Doggett T, Thebeau C, Zhang S, Semenkovich CF, Rajagopal R. Measurement of Energy Metabolism in Explanted Retinal Tissue Using Extracellular Flux Analysis. J Vis Exp. 2019; e58626.
https://doi.org/10.3791/58626 PMID:30663677

47. Nicholas D, Proctor EA, Raval FM, Ip BC, Habib C, Ritou E, Grammatopoulos TN, Steenkamp D, Dooms H, Apovian CM, Lauffenburger DA, Nikolajczyk BS. Advances in the quantification of mitochondrial function in primary human immune cells through extracellular flux analysis. PLoS One. 2017; 12:e0170975.
https://doi.org/10.1371/journal.pone.0170975
PMID:28178278

48. Lee JH, Liu R, Li J, Wang Y, Tan L, Li XJ, Qian X, Zhang C, Xia Y, Xu D, Guo W, Ding Z, Du L, et al. EGFR-Phosphorylated Platelet Isoform of Phosphofructokinase 1 Promotes PI3K Activation. Mol Cell. 2018; 70:197–210.e7.
https://doi.org/10.1016/j.molcel.2018.03.018
PMID:29677490

49. Marosi K, Bori Z, Hart N, Sárga L, Koltai E, Radák Z, Nyakas C. Long-term exercise treatment reduces oxidative stress in the hippocampus of aging rats. Neuroscience. 2012; 226:21–28.
https://doi.org/10.1016/j.neuroscience.2012.09.001
PMID:22982624

50. Lee JE, Kwon HJ, Choi J, Seo JS, Han PL. Aging increases vulnerability to stress-induced depression via upregulation of NADPH oxidase in mice. Commun Biol. 2020; 3:292.
https://doi.org/10.1038/s42003-020-1010-5
PMID:32504071

51. Wu SB, Wei YH. AMPK-mediated increase of glycolysis as an adaptive response to oxidative stress in human cells: implication of the cell survival in mitochondrial diseases. Biochim Biophys Acta. 2012; 1822:233–47.
https://doi.org/10.1016/j.bbadis.2011.09.014
PMID:22001850

52. Mowla SN, Lam EW, Jat PS. Cellular senescence and aging: the role of B-MYB. Aging Cell. 2014; 13:773–79.
https://doi.org/10.1111/acel.12242 PMID:24981831

53. Kim YY, Jee HJ, Um JH, Kim YM, Bae SS, Yun J. Cooperation between p21 and Akt is required for p53-dependent cellular senescence. Aging Cell. 2017; 16:1094–103.
https://doi.org/10.1111/acel.12639
PMID:28691365

54. Rizvi S, Raza ST, Mahdi F. Telomere length variations in aging and age-related diseases. Curr Aging Sci. 2014; 7:161–67.
https://doi.org/10.2174/1874609808666150122153151 PMID:25612739

55. Singulani MP, Stringhetta-Garcia CT, Santos LF, Morais SR, Louzada MJ, Oliveira SH, Chaves Neto AH, Dornelles RC. Effects of strength training on osteogenic differentiation and bone strength in aging female Wistar rats. Sci Rep. 2017; 7:42878.
https://doi.org/10.1038/srep42878
PMID:28211481

56. Li CJ, Cheng P, Liang MK, Chen YS, Lu Q, Wang JY, Xia ZY, Zhou HD, Cao X, Xie H, Liao EY, Luo XH. MicroRNA-188 regulates age-related switch between osteoblast and adipocyte differentiation. J Clin Invest. 2015; 125:1509–22.
https://doi.org/10.1172/JCI77716
PMID:25751060

57. Cho SJ, Moon JS, Lee CM, Choi AM, Stout-Delgado HW. Glucose Transporter 1-Dependent Glycolysis Is Increased during Aging-Related Lung Fibrosis, and Phloretin Inhibits Lung Fibrosis. Am J Respir Cell Mol Biol. 2017; 56:521–31.
https://doi.org/10.1165/rcmb.2016-0225OC
PMID:27997810

58. James EL, Michalek RD, Pitiyage GN, de Castro AM, Vignola KS, Jones J, Mohney RP, Karoly ED, Prime SS, Parkinson EK. Senescent human fibroblasts show increased glycolysis and redox homeostasis with extracellular metabolomes that overlap with those of irreparable DNA damage, aging, and disease. J Proteome Res. 2015; 14:1854–71.
https://doi.org/10.1021/pr501221g PMID:25690941

59. Wang D, Xiao Q, Zhang W, Wang X, Xue X, Zhang X, Yu Z, Zhao Y, Liu J, Wang H. Landscape of ubiquitination events that occur in host skin in response to tick (Haemaphysalis longicornis) bitten. Dev Comp Immunol. 2020; 104:103572.
https://doi.org/10.1016/j.dci.2019.103572
PMID:31838045

60. Dong DW, Srinivasan S, Guha M, Avadhani NG. Defects in cytochrome c oxidase expression induce a metabolic shift to glycolysis and carcinogenesis. Genom Data. 2015; 6:99–107.
https://doi.org/10.1016/j.gdata.2015.07.031
PMID:26697345

61. Moeller LC, Dumitrescu AM, Refetoff S. Cytosolic action of thyroid hormone leads to induction of hypoxia-inducible factor-1alpha and glycolytic genes. Mol Endocrinol. 2005; 19:2955–63.
https://doi.org/10.1210/me.2004-0542
PMID:16051672

62. Orang AV, Petersen J, McKinnon RA, Michael MZ. Micromanaging aerobic respiration and glycolysis in cancer cells. Mol Metab. 2019; 23:98–126.
https://doi.org/10.1016/j.molmet.2019.01.014
PMID:30837197

63. Jin K, Li L, Sun X, Xu Q, Song S, Shen Y, Deng X. Mycoepoxydiene suppresses HeLa cell growth by inhibiting glycolysis and the pentose phosphate pathway. Appl Microbiol Biotechnol. 2017; 101:4201–13.
https://doi.org/10.1007/s00253-017-8187-7
PMID:28224194

Supplementary Figures
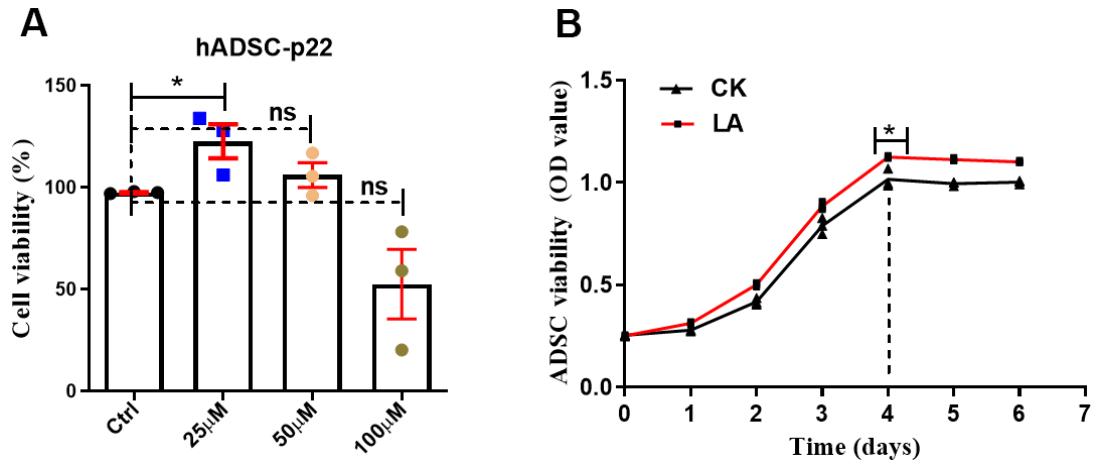
Supplementary Figure 1. Cell viability assay and survival curve analysis to monitor the effect of LA on aged hADSC. (**A**) Cell viability assay. (**B**) Survival curve. The data are presented as mean ± SD of three independent experiments. * p < 0.05, ** p < 0.01 compared to untreated cells.
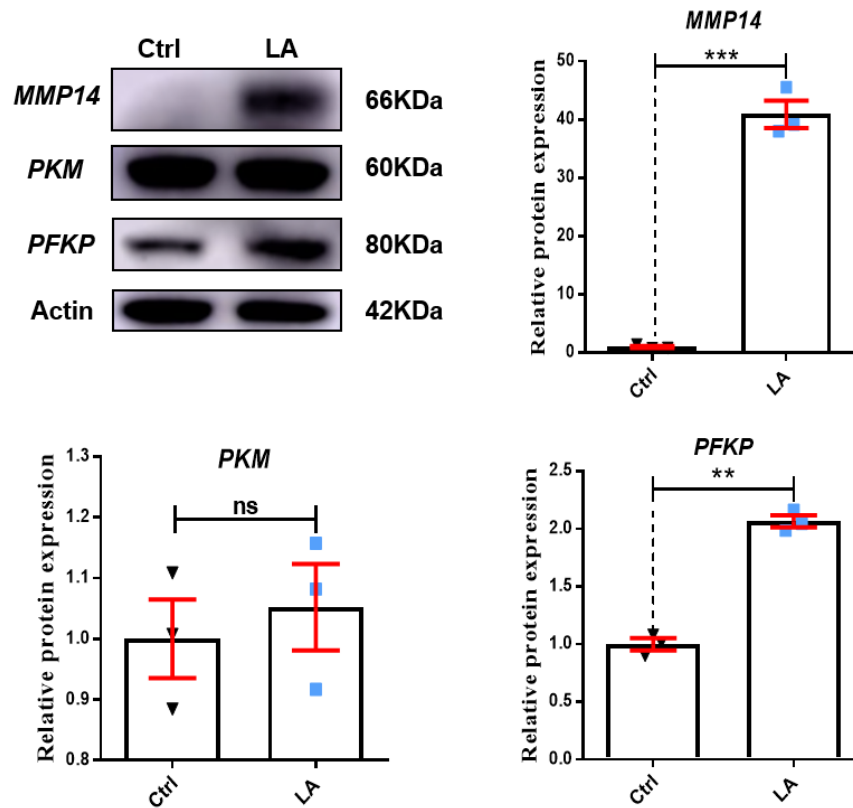
Supplementary Figure 2. Western blot analysis of glycolysis/gluconeogenesis signaling pathway related proteins in hADSCs treated as indicated. Data are presented as the mean ± SD of three independent experiments. *p < 0.05, **p < 0.01, ***p < 0.001 compared with untreated cells.

Supplementary Figure 3. Western blot analysis of AMPK protein in hADSCs treated as indicated (LA 24 h treatment). Data are presented as the mean ± SD of three independent experiments. *p < 0.05, **p < 0.01, ***p < 0.001 compared with untreated cells.

Supplementary Figure 4. Influences of LA on senescence of hADSCs can be reversed by glycolysis inhibitor 2-DG. (**A**) Western blot analysis of *AMPK* protein in hADSCs treated as indicated (LA treatment 80 h). (**B**) SA-β-gal staining of hADSCs (Scale bar: 100 μm) (LA treatment 48 h). The relative intensity of ROS was detected by a microplate reader. (**C**) qRT-PCR of mRNA levels of p16 gene (LA treatment 48 h). Data are presented as the mean ± SD of three independent experiments. *p < 0.05, **p < 0.01, ***p < 0.001 compared with control cells.